Research Article

Hyoung-Taek Lee, Hoyeol Lee, Jeonghoon Kim, Miju Park, Changhee Sohn and Hyeong-Ryeol Park*

Enhanced terahertz magneto-plasmonic effect enabled by epsilon-near-zero iron slot antennas

https://doi.org/10.1515/nanoph-2024-0665
Received November 22, 2024; accepted January 14, 2025;
published online February 17, 2025

Abstract: Terahertz magneto-plasmonics plays a crucial role in platforms for isolation and sensing applications, operating at terahertz frequencies. In spite of recent efforts to enhance magneto-optic effects using metasurfaces, the mechanism for optimizing these effects remains unclear in the terahertz regime. Here we investigate terahertz magneto-optic effects using 100 nm-thick iron slot antennas with varying widths, ranging from 20 μm to 300 nm. Interestingly, as the width of slot antenna decreases, this enhancement peaks around 1 μm, after which the effect diminishes for smaller widths. Based on the effective medium theory, the slot antennas exhibit a maximum Faraday rotation angle near the epsilon-near-zero region. Although the field enhancements in the slot become stronger with the sub-micron widths, the magneto-optic effect may decrease with increasing effective dielectric constant due to gap plasmon effects in the sub-micron region. Our findings provide essential criteria for designing ferromagnetic metasurfaces with enhanced Faraday rotations at terahertz frequencies.

Keywords: terahertz metasurface; terahertz magneto-optics; epsilon-near-zero; Faraday rotation; gap plasmon effect; effective dielectric constant

Hyoung-Taek Lee and Hoyeol Lee contributed equally to this work.

***Corresponding author: Hyeong-Ryeol Park**, Department of Physics, Ulsan National Institute of Science and Technology (UNIST), Ulsan 44919, Republic of Korea, E-mail: nano@unist.ac.kr.
https://orcid.org/0000-0002-6586-9466
Hyoung-Taek Lee, Department of Physics, Ulsan National Institute of Science and Technology (UNIST), Ulsan 44919, Republic of Korea; and Pohang Accelerator Laboratory, POSTECH, Pohang 37673, Republic of Korea. https://orcid.org/0000-0002-7180-7114
Hoyeol Lee, **Jeonghoon Kim**, **Miju Park and Changhee Sohn**, Department of Physics, Ulsan National Institute of Science and Technology (UNIST), Ulsan 44919, Republic of Korea.
https://orcid.org/0009-0004-4722-0585 (H. Lee).
https://orcid.org/0009-0003-5608-6640 (J. Kim).
https://orcid.org/0000-0002-5387-4348 (M. Park).
https://orcid.org/0000-0002-5043-497X (C. Sohn)

1 Introduction

Plasmonics enables the manipulation of light by structuring materials at the nanoscale to control light-matter interactions effectively [1]–[3]. In the terahertz (THz) regime, the resonant behaviors of slot antennas are explained by localized surface plasmons (LSPs) [4], [5], and the resonance of the slot antennas is determined by the shape of the slot antenna. Magneto-Optical (MO) effects, such as Faraday and Kerr rotations, could be enhanced by plasmonic structures, and this is so-called magneto-plasmonics [6]–[11]. The MO effect enhanced by plasmonic structures has been utilized in applications such as optical isolation and sensing [12]–[17]. The MO enhancement has largely been studied in the visible and near-infrared regions, where MO effects are typically driven by interband transitions [18]–[22]. However, ferromagnetic metals, unlike noble metals such as Au and Ag, often exhibit high losses for surface plasmon-polaritons in the visible range, which limits their ability to achieve strong enhancements [23]–[26].

Enhanced MO effects are also required in the THz regime, where the needs for isolator systems and sensing platforms are similar to those in the visible spectrum [27]–[31]. In the THz range, the optical conductivity of ferromagnetic metals is typically comparable to that of noble metals, despite the fact that their optical conductivity is relatively low. As a result, ferromagnetic metals can be utilized to develop multifunctional plasmonic metasurfaces that incorporate both noble-metal-like performances and ferromagnetic properties. By structuring ferromagnetic materials to tailor their optical response to the external magnetic fields, one can enhance MO effects and facilitate effective light-matter interactions [23], [32]–[35]. For example, a prior work has shown that circular hole patterned Co films enhanced Kerr rotation in the THz range, which is a reflective MO effect [36]. However, the mechanism in detail for maximizing THz magneto-plasmonic enhancements has not yet been fully understood despite these findings and substantial research efforts [27], [28], [37], [38].

In this study, we investigate how THz metasurfaces, such as slot antennas, patterned in ferromagnetic films influence enhancement of MO effects in the THz range.

Specifically, we observe a transmission-type MO effect, Faraday rotation, through slot antennas patterned in an iron film. To realize this, iron slot antennas with varying its widths were fabricated using electron beam lithography and lift-off processes. The fabricated iron slot antennas were experimentally characterized by a transmission-type terahertz time-domain spectroscopy (THz-TDS) [39]. The effective medium of the ferromagnetic slot antennas can exhibit epsilon-near-zero (ENZ) properties, where the real part of the diagonal term of the dielectric function approaches zero near the peak position in the transmission spectrum. It has been demonstrated in the telecommunication wavelength range that MO effects can be significantly enhanced near this ENZ region [40]. In our results, the largest Faraday rotation angle was observed near the peak position in the spectrum, and interestingly, the angle increased as the width of the slot decreased, reaching a maximum at a 1 μm width, even though the Faraday rotation angle decreased when the width reduced to less than 1 μm. This phenomenon arises from the increased effective dielectric constant of the environments surrounding the slot antenna as the slot width decreases, enabled by the gap plasmon effect. Our results offer criteria for optimizing THz MO effects and provide important guidance in the design of magneto-plasmonic metasurfaces at THz frequencies.

2 Results and discussion

As shown in Figure 1, the ferromagnetic Fe film was patterned with slot antenna arrays with the slot widths a_x, ranging from 20 μm to 300 nm, the slot length a_y of 50 μm, the horizontal period l_x of 73 μm, and the vertical period l_y of 83 μm. The resonance frequency of the slot antenna primarily depends on the slot length a_y [41]–[43]. The structural parameters of the slot antenna were designed to obtain the maximum THz transmittance with the highest Q-factor at near 1 THz using an inverse design based on deep learning algorithms [44], in order to avoid overlap between the peak and dip positions on the transmittance spectrum. In Figure 1a–d, we have shown how the slot antennas were patterned using electron beam lithography, followed by the deposition of a 100 nm thick Fe film using an electron beam evaporator, and fabricated using lift-off process (see the details in the Methods section). In Figure 1e–k, scanning electron

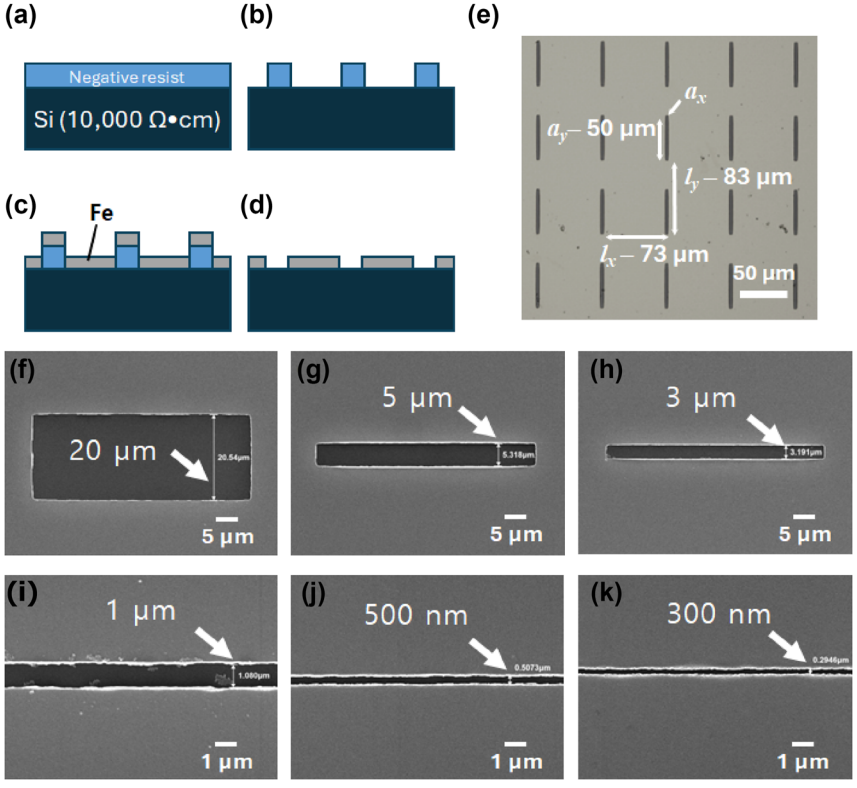

Figure 1: Fabrication of iron slot antennas using electron beam lithography. (a) A 500 nm-thick negative resist is spin-coated on Si substrate. (b) The resist pattern is completed through electron beam lithography and develop processes. (c) Fe 100 nm/Cr 5 nm is deposited using an electron beam evaporator. (d) The slot antennas were fabricated by removing the resist through a lift-off process. (e) The optical microscopy image of the slot antenna array. a_x is the width of slot, a_y is the length of slot, l_x is the period along the *x*-axis, and l_y is the period along the *y*-axis. (f–k) Scanning electron microscope (SEM) images of slot antenna patterns with the widths of (f) 20 μm, (g) 5 μm, (h) 3 μm, (i) 1 μm, (j) 500 nm, and (k) 300 nm, respectively.

microscope (SEM) images of the slot antennas are presented, showing that the desired widths have been achieved. As shown in Supplementary material S1, the X-ray diffraction (XRD) analysis of the deposited bare iron film indicates that it is amorphous, and the magnetoresistance measurement reveals an out-of-plane coercive field of 84.4 mT.

When x-polarized light passes through a ferromagnetic material along the z-axis, it can experience Faraday rotation, causing y-polarization. In this case, the dielectric constant of the ferromagnetic material can be expressed in the form of a tensor with off-diagonal terms as follows:

$$\epsilon_{\mathrm{Fe}} = \begin{pmatrix} \epsilon_{xx} & \epsilon_{xy} & 0 \\ -\epsilon_{yx} & \epsilon_{yy} & 0 \\ 0 & 0 & \epsilon_{zz} \end{pmatrix}$$

where the diagonal terms of $\epsilon_{xx} = \epsilon_{yy} = \epsilon_{zz}$ are isotropic dielectric constant. When an external magnetic field is applied in the z-direction, the magneto-optical material exhibits an off-diagonal term, $\epsilon_{xy} = \epsilon_{yx}$. It should be noted that the film remains structurally isotropic; however, the dielectric tensor is influenced by the MO effect induced by the external magnetic field. When an external magnetic field is not applied, the diagonal terms are maintained, but the off-diagonal terms become zero.

In Figure 2a, we performed transmission-type THz-TDS to determine how much the polarization of transmitted light through the iron slot antennas rotated compared to the incident x-polarized light. Especially, the detector crystal of ZnTe was mounted on a motorized rotator to directly measure its polarization rotation [45]–[47]. Before mounting the sample, the photo-conductive antenna and the ZnTe detector were aligned to the maximum at 0°, and then the sample was mounted and aligned precisely. After that, each sample was measured by rotating the motorized rotator with detection crystal between −20 and +10° with intervals of 2°. As a result of comparing the peak amplitude at each angle with and without an external magnetic field, the Faraday rotation angle was determined (see the details in the Faraday rotation analysis of Supplementary material S2). The

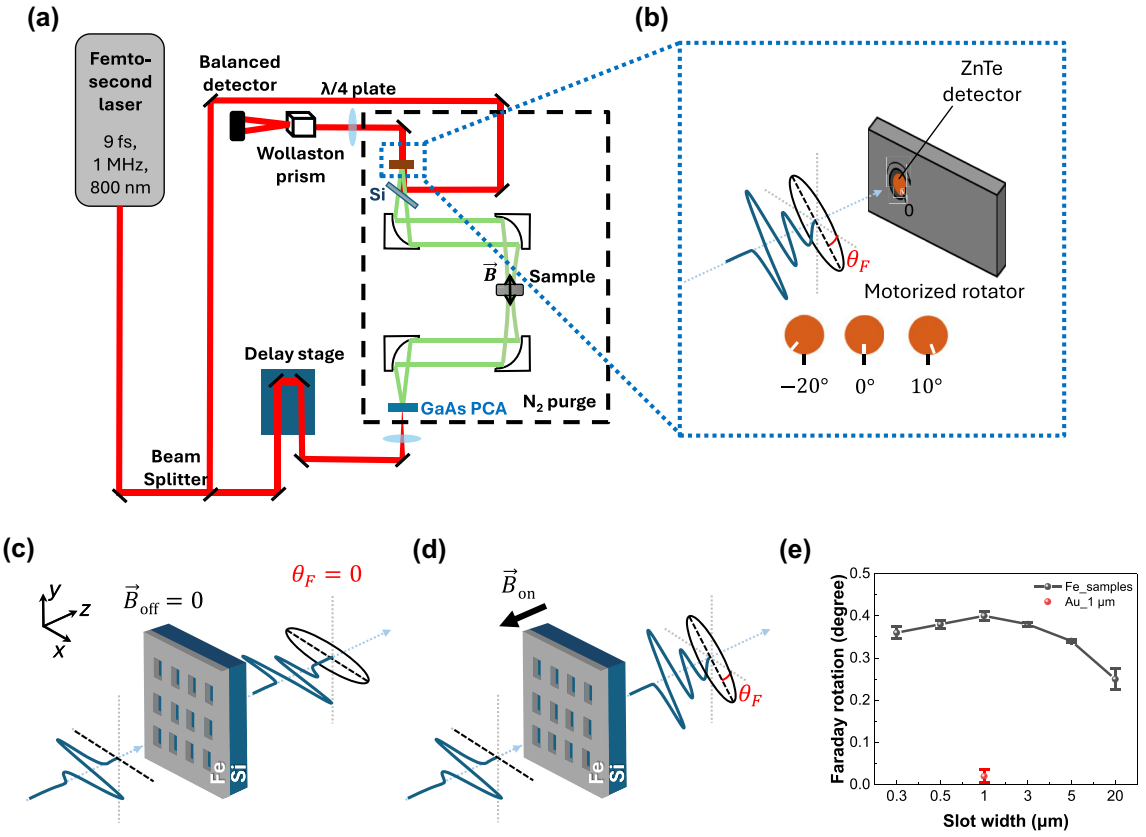

Figure 2: Experimental method for Faraday rotation measurement. (a) Schematic of a conventional THz-TDS setup. A femtosecond Ti:sapphire laser with a wavelength of 800 nm and up to 4 W output power excites a photoconductive antenna that generates THz pulses. (b) The THz pulse travels through the sample is detected by a ZnTe detector mounted on a motorized rotator. (c–d) Schematic of Faraday rotation effect by the iron slot antennas (c) without and (d) with an external magnetic field, where θ_F is the Faraday rotation angle. (e) Measured Faraday rotation angles of the iron (Fe) slot antennas with the varying widths between 0.3 and 20 μm are compared with the Faraday rotation of gold (Au) slot antennas with the width of 1 μm.

sample was placed on a 3 mm × 3 mm aperture, and an out-of-plane magnetic field of approximately 90 mT was applied using a donut-shaped neodymium magnet (Figures 2c and d).

The measured Faraday rotation angles, as shown in Figure 2e and Table 1, demonstrate the a_x-dependent enhancement of the MO effect. As the slot width decreases, the Faraday rotation continues to increase until the width reaches 1 μm, demonstrating significant improvement. The Faraday rotation angle is enhanced by approximately 160 % when comparing the results for the width of 1 μm to the width of 20 μm. This enhancement may be due to the strong light-matter interaction confined within sub-wavelength structures [48]–[50]. It is interesting, however, to note that the enhancement tends to decrease as slot widths decrease below 1 μm. This behavior illustrates that while reducing the gap size up to a certain threshold improves MO response, going below that threshold (especially down to the nanometer scale) introduces additional physical phenomena that can hinder performance, including strong plasmonic absorption or field localization that confines energy too tightly.

The gold slot antenna at $a_x = 1$ μm exhibited a Faraday rotation angle close to zero within the margin of error, which was about 20 times smaller than that of the patterned Fe film samples. Furthermore, when we compare the unpatterned Fe film with the patterned Fe film, the iron exhibits extremely high conductivity in the THz range, resulting in a transmitted electric field amplitude of less than 1 % even for thin films of 50 nm [51]. In such cases, the transmitted amplitude is too low to distinguish differences in angle dependence. The experimental results in Supplementary material S3 contain the measured peak amplitudes for each sample with all rotation angles of the ZnTe detector, and it demonstrates the challenges in determining the Faraday rotation angle in the bare Fe film. It should be noted that as a result of patterning the bare Fe film, it will be possible to measure the Faraday rotation angle, which was difficult to measure with a transmission-type THz setup.

Table 1: A table of the Faraday rotation angles measured for the Fe slot antennas with the varying widths between 0.3 and 20 μm and the Au slot antennas with the width of 1 μm.

Samples	Faraday rotation angle
Au, $a_x = 1$ μm	0.02°
Fe, $a_x = 20$ μm	0.25°
Fe, $a_x = 5$ μm	0.34°
Fe, $a_x = 2$ μm	0.38°
Fe, $a_x = 1$ μm	0.4°
Fe, $a_x = 0.5$ μm	0.38°
Fe, $a_x = 0.3$ μm	0.36°

For a more detailed understanding of the slot width-dependent Faraday rotation angles, we compared transmitted amplitude spectra of the Fe slot antennas with varying widths when the magnetic field is on and off, using the THz-TDS experiments (Figure 3a). To verify the MO effects induced by the off-diagonal term in the dielectric function of ferromagnetic Fe film, we reproduced the MO effect with and without the magnetic field using full-wave optical simulations, as shown in Figure 3b (see the details of the numerical simulation in Methods) [52]. The simulation results are in good qualitative agreement with the experimental results. The observed resonance behavior and enhancement of MO effects can be attributed to LSPs, that cause the charge distribution and current flow within the slot antenna. The slight difference between transmitted amplitudes in the experiments (Figure 3a) and the simulations (Figure 3b) is attributed to stitching errors during the e-beam lithography process. Due to the diffraction limit of UV light, nanometer-scale patterning is difficult to achieve using photolithography. A large area of 5 mm × 5 mm is patterned using e-beam lithography, which can pattern only 400 μm × 400 μm at one position of the sample stage. This stitching error that occurs when moving from one position to the neighbor position, leads to broader spectral features and lower peak amplitude (see the details of stitching errors in Supplementary material S4).

Figure 3c illustrates the maximum changes due to switching on and off the magnetic field for each sample, with the largest difference near the peak position. Furthermore, the MO effect has been enhanced as the slot width decreases down to 1 μm. Interestingly, however, we observed that with even smaller widths of a few hundred nanometers, the enhancement of the Δt_{res} diminishes. The reason why the Δt_{res} is maximized at 1 μm width will be discussed later. In Figure 3c, the experimentally observed Δt_{res} of approximately 8 % at 1 μm sample requires an angle of $\theta = \cos^{-1}(0.92) = 23°$. This is significantly larger than the relatively small Faraday rotation angle of 0.4°. When the dielectric tensor includes the off-diagonal term, it can influence the diagonal terms of the refractive index. As a result, Δt_{res} observed is greater than what would be expected solely based on the Faraday rotation angle. The absorbance of the slot antenna in Figure 3c was obtained through simulations under zero magnetic field (For the details of absorbance and absorption coefficient spectra, see the Supplementary material S5). Interestingly, the absorbance reaches its maximum value at the slot width of 1 μm, due to plasmonic

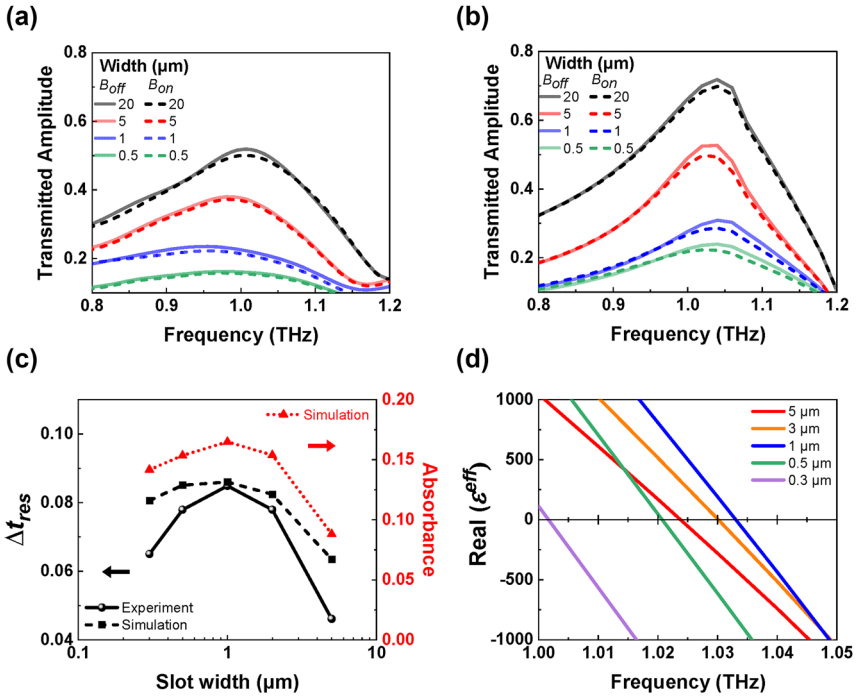

Figure 3: Transmitted amplitude spectra and magneto-optical enhancement of Fe slot antennas. (a) Measured and (b) simulated transmitted amplitude spectra of the Fe slot antennas with the varying slot widths when the magnetic field is on and off ($\vec{B}_{on}$ and $\vec{B}_{off}$). (c) The normalized peak amplitude difference, $\Delta t_{res} = \left|t_{res}^{on} - t_{res}^{off}\right| / t_{res}^{off}$, and the absorbance as a function of slot width. Here, t_{res}^{on} and t_{res}^{off} are the resonant peak amplitudes with and without the external magnetic field, respectively. The absorbance is calculated using the formula $1 - T - R$, where T and R represent the transmittance and the reflectance without the external magnetic field. (d) The real part of the dielectric constants of the effective medium (ϵ^{eff}) with the varying widths as a function of frequency. It reveals the occurrence of an epsilon-near-zero (ENZ) region near the peak position.

absorption by the slot antenna that results in a giant Faraday rotation effect [19], [53].

Using the effective medium theory to model the Fe slot antennas as a single film, the dielectric constant of the effective medium can be derived by analyzing the transmitted amplitude and phase information from the simulations. Details on extracting the dielectric constant from the effective medium (ϵ^{eff}) are provided in Supplementary material S6, with Figure 3d showing the real part of ϵ^{eff} as a function of frequency. It is noted that the real part of the ϵ^{eff} approaches zero near the peak position. An earlier work [40] also showed that MO effects are most significantly enhanced in the vicinity of the ENZ region. Furthermore, the ENZ region of the effective medium at the width of 1 μm appears at the highest frequency, which might explain why the MO effect has been maximized with the 1 μm width slot.

Due to the unintuitive behavior appearing at the hundred nanometers widths, we focus on the peak position as it varies with the width of the iron slot antenna when no magnetic field is applied. Here, the slot antenna is not considered as an effective medium. Instead, we analyze it from the perspective of the effective index of the surrounding materials, including air and the substrate. It is important to note that, according to antenna theory, the peak position is primarily determined by the vertical length of the rectangular hole, a_y [41], [42]. However, small variations in the effective index surrounding the slot antenna due to the width, a_x, can also induce changes in the peak position. According to the experimental results in Figure 4a, for samples wider than 1 μm, a blue shift occurs as the width decreases, whereas for samples narrower than 1 μm, a red shift is observed as the width decreases. The simulation results for more slot widths in Figure 4b show a similar shift in peak position. The dielectric constant of the material surrounding the slot antenna influences the resonant feature of the antenna [41]. When the slot width is even smaller than the wavelength, the gap plasmon effect will become non-negligible, causing the resonance peak shift [54], [55]. Actually, in the widths between 1 and 10 μm, the MO effect continues to be enhanced, while the decreasing effective index causes a blue shift in the peak position. Interestingly, the peak shift changes to a red shift at below 1 μm where the gap plasmon effect occurs, and the MO effect diminishes. Based on our findings, we conclude that when the effective dielectric constant of the environmental material surrounding the slot antenna is lowest, the Faraday rotation angle is enhanced the most.

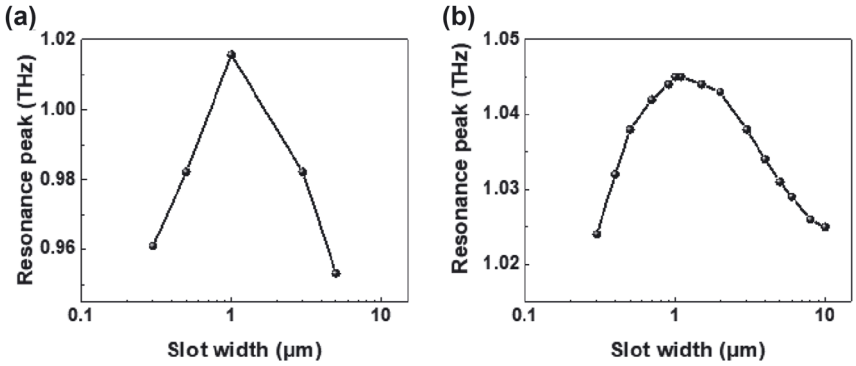

Figure 4: Resonance peak positions as a function of the slot width are shown in (a) the experiments and (b) the simulations.

3 Conclusions

We experimentally demonstrate that the magneto-plasmonic effect of iron slot antennas can be significantly enhanced through precise structural manipulation of ferromagnetic iron films at the THz region. By varying slot widths and applying an external magnetic field, we achieved an approximately 160 % increase in the Faraday rotation angle with the slot width of 1 μm compared to larger gaps. This finding emphasizes the potential of structural manipulation to improve magneto-plasmonics performance effectively. An effective medium analysis revealed that the peak magneto-plasmonics response occurred near the ENZ region, which is critical when considering magneto-plasmonics enhancements. Under magnetic field on/off conditions, both experimental and simulation results showed that the enhancement of the magneto-plasmonic effect was most pronounced at the width of 1 μm. Further reduction below this threshold, however, presented limitations, possibly resulting from an increase in the effective dielectric constant of the environmental materials surrounding the slot due to the gap plasmon effect. Our findings demonstrate that optimizing structural parameters, particularly the effective dielectric constant within the slot, plays a critical role in maximizing the magneto-plasmonic effect. This work highlights the potential for tailored ferromagnetic film patterning to advance magneto-plasmonic applications in the THz regime, offering insights for further optimization.

4 Methods

Fabrications. The ferromagnetic Fe slot antennas were fabricated using electron beam lithography. First, a negative electron beam resist (MA-N 2405) is spin-coated with a 500 nm thickness on a 500 μm-thick undoped silicon substrate. After spin-coating, samples are baked on the hot plate at 90 °C for 1 min 20 s. As the next step, the electron beam is illuminated on the electron beam resist at 100 μC/cm^2 at an acceleration voltage of 30 keV. Subsequently, the 100 nm iron film was deposited with 5 nm Cr adhesion layer on the samples using electron beam evaporation. Finally, the lift-off process is performed to remove the electron beam resist, and the Fe slot antenna arrays are completed.

Simulations. The full-wave optical simulations were performed to analyze the transmitted amplitude spectra of the Fe slot antennas using the finite element method (COMSOL Multiphysics, wave optics module). The Fe slot antennas with a thickness of 100 nm on a silicon substrate has the following parameters: horizontal length (or slot width) of rectangular hole of a_x: 0.3–20 μm, vertical length of rectangular hole of a_y: 50 μm, x-periodicity of l_x: 73 μm, and y-periodicity of l_y at 83 μm. The refractive index of the air inside and above the slot is 1.0, while the refractive index of the silicon substrate below the slot is 3.4. The diagonal term of the dielectric function of the Fe film was obtained using the Drude model [56]. as follows:

$$\tilde{\epsilon}_{xx}(\omega) = \tilde{\epsilon}_{yy}(\omega) = \tilde{\epsilon}_{zz}(\omega) = \epsilon_\infty - \frac{\omega_p^2}{\omega^2 + i\omega\omega_\tau}$$

where $\omega_p = 0.622 \times 10^4$ THz and $\omega_\tau = 27.7$ THz are the Drude parameters of a bulk iron [56]. When the external magnetic field is applied to the iron slot antennas, we used the off-diagonal terms of the following fitting parameters: $\epsilon_{xy} = \epsilon_{yx} = 0.45i \cdot \epsilon_{xx}$, which was selected based on our experimental results. The perfectly matched layers were applied to the top and bottom of the simulation region to prevent unwanted reflections. Periodic boundary conditions were applied to the *xz*- and *yz*-boundaries. To process the significant computational load due to the thin thickness of the pattern, a quarter geometry was used, and adaptive meshing was applied.

Acknowledgements: We thank UCRF (UNIST Central Research Facilities) for support of using the equipment.
Research funding: This work was supported by the National Research Foundation (NRF) of Korea Government (MSIT: 2022M3H4A1A04096465, 2023K2A9A1A0109872811, RS-2024-00444182, RS-2024-00348920, and RS-2024-00353252) and the Republic of Korea's MSIT (Ministry of Science and ICT) under the ITRC (Information Technology Research Center) support program (IITP-2023-RS-2023-00259676) supervised by the IITP (Institute of Information and Communications Technology Planning & Evaluation).
Author contributions: HTL and HRP conceived the idea and designed the research. HTL took the simulations. HL fabricated the samples. HL and JK conducted the terahertz time-domain spectroscopy measurement. MP and CS characterized the iron film. HRP supervised the project. All authors participated in the discussions of the results, wrote the manuscript together, and accepted responsibility for the entire content of this manuscript and approved its submission.
Conflict of interest: Authors state no conflict of interests.
Data availability: Data sharing is not applicable to this article as no datasets were generated or analyzed during the current study.

References

[1] J. A. Schuller, E. S. Barnard, W. S. Cai, Y. C. Jun, J. S. White, and M. L. Brongersma, "Plasmonics for extreme light concentration and manipulation," *Nat. Mater.*, vol. 9, no. 3, pp. 193—204, 2010.
[2] S. M. Chen, G. X. Li, K. W. Cheah, T. Zentgraf, and S. Zhang, "Controlling the phase of optical nonlinearity with plasmonic metasurfaces," *Nanophotonics*, vol. 7, no. 6, pp. 1013—1024, 2018.
[3] T. T. Kang, *et al*., "Large-scale, power-efficient Au/VO active metasurfaces for ultrafast optical modulation," *Nanophotonics*, vol. 10, no. 2, pp. 909—918, 2021.
[4] J. W. Lee, *et al*., "Shape resonance omni-directional terahertz filters with near-unity transmittance," *Opt. Express*, vol. 14, no. 3, pp. 1253—1259, 2006.
[5] J. H. Kang, D. S. Kim, and M. Seo, "Terahertz wave interaction with metallic nanostructures," *Nanophotonics*, vol. 7, no. 5, pp. 763—793, 2018.
[6] R. Fujikaw, A. V. Baryshev, J. Kim, H. Uchida, and M. Inoue, "Contribution of the surface plasmon resonance to optical and magneto-optical properties of a Bi:YIG-Au nanostructure," *J. Appl. Phys.*, vol. 103, no. 7, 2008. https://doi.org/10.1063/1.2829036.
[7] B. L. Johnson and H. H. Shiau, "Guided magneto-plasmon polaritons in thin films: Non-reciprocal propagation and forbidden modes," *J. Phy. Condens. Matter*, vol. 20, no. 33, 2008. https://doi.org/10.1088/0953-8984/20/33/335217.
[8] G. A. Wurtz, *et al*., "Controlling optical transmission through magneto-plasmonic crystals with an external magnetic field," *New J. Phys.*, vol. 10, no. 10, 2008. https://doi.org/10.1088/1367-2630/10/10/105012.
[9] G. Ctistis, E. Papaioannou, P. Patoka, J. Gutek, P. Fumagalli, and M. Giersig, "Optical and magnetic properties of hexagonal arrays of subwavelength holes in optically thin cobalt films," *Nano Lett.*, vol. 9, no. 1, pp. 1—6, 2009.
[10] B. Sepúlveda, J. B. González-Díaz, A. García-Martín, L. M. Lechuga, and G. Armelles, "Plasmon-induced magneto-optical activity in nanosized gold disks," *Phys. Rev. Lett.*, vol. 104, no. 14, 2010. https://doi.org/10.1103/PhysRevLett.104.147401.
[11] V. I. Belotelov, *et al*., "Enhanced magneto-optical effects in magnetoplasmonic crystals," *Nat. Nanotechnol.*, vol. 6, no. 6, pp. 370—376, 2011.
[12] G. Armelles, A. Cebollada, A. García-Martín, and M. U. González, "Magnetoplasmonics: Combining magnetic and plasmonic functionalities," *Adv. Opt. Mater.*, vol. 1, no. 1, pp. 10—35, 2013.
[13] G. Armelles, *et al*., "Magnetic field modulation of chirooptical effects in magnetoplasmonic structures," *Nanoscale*, vol. 6, no. 7, pp. 3737—3741, 2014.
[14] M. W. Song, *et al*., "Color display and encryption with a plasmonic polarizing metamirror," *Nanophotonics*, vol. 7, no. 1, pp. 323—331, 2018.
[15] J. Y. Zhou, *et al*., "Portable tumor biosensing of serum by plasmonic biochips in combination with nanoimprint and microfluidics," *Nanophotonics*, vol. 8, no. 2, pp. 307—316, 2019.
[16] Y. T. Lin, A. Hassanfiroozi, W. R. Jiang, M. Y. Liao, W. J. Lee, and P. C. Wu, "Photoluminescence enhancement with all-dielectric coherent metasurfaces," *Nanophotonics*, vol. 11, no. 11, pp. 2701—2709, 2022.
[17] Z. Zheng, *et al*., "Advances in nonlinear metasurfaces for imaging, quantum, and sensing applications," *Nanophotonics*, vol. 12, no. 23, pp. 4255—4281, 2023.
[18] J. L. Erskine and E. A. Stern, "Calculation of M23 magneto-optical absorption-spectrum of ferromagnetic nickel," *Phys. Rev. B*, vol. 12, no. 11, pp. 5016—5024, 1975.
[19] J. Y. Chin, *et al*., "Nonreciprocal plasmonics enables giant enhancement of thin-film Faraday rotation," *Nat. Commun.*, vol. 4, no. 1, 2013. https://doi.org/10.1038/ncomms2609.
[20] G. M. Wysin, V. Chikan, N. Young, and R. K. Dani, "Effects of interband transitions on Faraday rotation in metallic nanoparticles," *J. Phy. Condens. Matter*, vol. 25, no. 32, 2013. https://doi.org/10.1088/0953-8984/25/32/325302.
[21] P. E. Zimnyakova, *et al*., "Two-dimensional array of iron-garnet nanocylinders supporting localized and lattice modes for the broadband boostedmagneto-optics," *Nanophotonics*, vol. 11, no. 1, pp. 119—127, 2022.
[22] F. F. Zhang, T. Atsumi, X. L. Xu, S. Murai, and K. Tanaka, "Tunable Faraday rotation of ferromagnet thin film in whole visible region coupled with aluminum plasmonic arrays," *Nanophotonics*, vol. 11, no. 2, pp. 275—288, 2022.
[23] M. A. Ordal, *et al*., "Optical-properties of the metals Al, Co, Cu, Au, Fe, Pb, Ni, Pd, Pt, Ag, Ti, and W in the infrared and far infrared," *Appl. Opt.*, vol. 22, no. 7, pp. 1099—1119, 1983.
[24] C. Hermann, V. A. Kosobukin, G. Lampel, J. Peretti, V. I. Safarov, and P. Bertrand, "Surface-enhanced magneto-optics in metallic multilayer films," *Phys. Rev. B*, vol. 64, no. 23, 2001. https://doi.org/10.1103/PhysRevB.64.235422.
[25] B. Sepúlveda, L. A. Lechuga, and G. Armelles, "Magnetooptic effects in surface-plasmon-polaritons slab waveguides," *J. Light. Technol.*, vol. 24, no. 2, pp. 945—955, 2006.

[26] V. I. Belotelov, *et al*., "Plasmon-mediated magneto-optical transparency," *Nat. Commun.*, vol. 4, no. 1, 2013. https://doi.org/10.1038/ncomms3128.
[27] Q. Y. Mu, F. Fan, Y. Y. Ji, J. R. Cheng, and S. J. Chang, "Enhanced terahertz magneto-optical Kerr rotation based on metasurface structure," *Opt. Commun.*, vol. 460, no. 1, 2020. https://doi.org/10.1016/j.optcom.2019.125163.
[28] F. Fan, C. Z. Zhong, Z. Y. Zhang, S. S. Li, and S. J. Chang, "Terahertz chiral sensing and magneto-optical enhancement for ferromagnetic nanofluids in the chiral metasurface," *Nanoscale Adv.*, vol. 3, no. 16, pp. 4790—4798, 2021.
[29] Z. Y. Tan, F. Fan, D. Zhao, S. S. Li, X. H. Wang, and S. J. Chang, "Linear-polarized terahertz isolator by breaking the gyro-mirror symmetry in cascaded magneto-optical metagrating," *Nanophotonics*, vol. 10, no. 16, pp. 4141—4148, 2021.
[30] Z. Q. Zhang, R. Zhao, M. Y. Cong, and J. F. Qiu, "Developments of terahertz metasurface biosensors: A literature review," *Nanotechnol. Rev.*, vol. 13, no. 1, 2024, Art. no. 20230182.
[31] Y. Lu, *et al*., "Nonlinear optical physics at terahertz frequency," *Nanophotonics*, vol. 13, no. 18, pp. 3279—3298, 2024.
[32] M. Diwekar, V. Kamaev, J. Shi, and Z. V. Vardeny, "Optical and magneto-optical studies of two-dimensional metallodielectric photonic crystals on cobalt films," *Appl. Phys. Lett.*, vol. 84, no. 16, pp. 3112—3114, 2004.
[33] J. B. González-Díaz, B. Sepúlveda, A. García-Martín, and G. Armelles, "Cobalt dependence of the magneto-optical response in magnetoplasmonic nanodisks," *Appl. Phys. Lett.*, vol. 97, no. 4, 2010. https://doi.org/10.1063/1.3474617.
[34] V. Bonanni, *et al*., "Designer magnetoplasmonics with nickel nanoferromagnets," *Nano Lett.*, vol. 11, no. 12, pp. 5333—5338, 2011.
[35] N. Kostylev, I. S. Maksymov, A. O. Adeyeye, S. Samarin, M. Kostylev, and J. F. Williams, "Plasmon-assisted high reflectivity and strong magneto-optical Kerr effect in permalloy gratings," *Appl. Phys. Lett.*, vol. 102, no. 12, 2013. https://doi.org/10.1063/1.4798657.
[36] B. Gupta, S. Pandey, A. Nahata, B. Sensale-Rodriguez, S. Guruswamy, and A. Nahata, "Terahertz magneto-plasmonics using cobalt subwavelength aperture arrays," *Sci. Rep.*, vol. 7, no. 1, 2017. https://doi.org/10.1038/s41598-017-12369-5.
[37] M. Shalaby, M. Peccianti, Y. Ozturk, and R. Morandotti, "A magnetic non-reciprocal isolator for broadband terahertz operation," *Nat. Commun.*, vol. 4, no. 1, 2013. https://doi.org/10.1038/ncomms2572.
[38] T. J. Huisman, *et al*., "Terahertz magneto-optics in the ferromagnetic semiconductor HgCdCrSe," *Appl. Phys. Lett.*, vol. 106, no. 13, 2015. https://doi.org/10.1063/1.4916884.
[39] J. Neu and C. A. Schmuttenmaer, "Tutorial: An introduction to terahertz time domain spectroscopy (THz-TDS)," *J. Appl. Phys.*, vol. 124, no. 23, 2018. https://doi.org/10.1063/1.5047659.
[40] K. Ikeda, T. J. Liu, Y. Ota, N. Kobayashi, and S. Iwamoto, "Enhanced magneto-optical effects in epsilon-near-zero indium tin oxide at telecommunication wavelengths," *Adv. Opt. Mater.*, vol. 12, no. 2, 2024. https://doi.org/10.1002/adom.202301320.
[41] F. J. García-Vidal, E. Moreno, J. A. Porto, and L. Martín-Moreno, "Transmission of light through a single rectangular hole," *Phys. Rev. Lett.*, vol. 95, no. 10, 2005. https://doi.org/10.1103/PhysRevLett.95.103901.
[42] J. Bravo-Abad, L. Martín-Moreno, and F. J. García-Vidal, "Resonant transmission of light through subwavelength holes in thick metal films," *IEEE J. Sel. Top. Quantum Electron.*, vol. 12, no. 6, pp. 1221—1227, 2006.
[43] H. R. Park, *et al*., "Resonance behavior of single ultrathin slot antennas on finite dielectric substrates in terahertz regime," *Appl. Phys. Lett.*, vol. 96, no. 21, 2010. https://doi.org/10.1063/1.3437091.
[44] H. T. Lee, J. Kim, and H. R. Park, "Rapid inverse design of high Q-factor terahertz filters [Invited]," *Opt. Mater. Express*, vol. 13, no. 11, pp. 3384—3393, 2023.
[45] Q. Wu, M. Litz, and X. C. Zhang, "Broadband detection capability of ZnTe electro-optic field detectors," *Appl. Phys. Lett.*, vol. 68, no. 21, pp. 2924—2926, 1996.
[46] C. M. Morris, R. V. Aguilar, A. V. Stier, and N. P. Armitage, "Polarization modulation time-domain terahertz polarimetry," *Opt. Express*, vol. 20, no. 11, pp. 12303—12317, 2012.
[47] D. K. George, A. V. Stier, C. T. Ellis, B. D. McCombe, J. Cerne, and A. G. Markelz, "Terahertz magneto-optical polarization modulation spectroscopy," *J. Opt. Soc. Am. B*, vol. 29, no. 6, pp. 1406—1412, 2012.
[48] J. Jeong, D. S. Kim, and H. R. Park, "Beyond-hot-spot absorption enhancement on top of terahertz nanotrenches," *Nanophotonics*, vol. 11, no. 13, pp. 3159—3167, 2022.
[49] G. S. Ji, *et al*., "Terahertz virus-sized gold nanogap sensor," *Nanophotonics*, vol. 12, no. 1, pp. 147—154, 2023.
[50] H. T. Lee, J. Kim, J. S. Lee, M. Yoon, and H. R. Park, "More than 30 000-fold field enhancement of terahertz nanoresonators enabled by rapid inverse design," *Nano Lett.*, vol. 23, no. 24, pp. 11685—11692, 2023.
[51] H. T. Lee, *et al*., "Measuring complex refractive indices of a nanometer-thick superconducting film using terahertz time-domain spectroscopy with a 10 femtoseconds pulse laser," *Crystals*, vol. 11, no. 6, 2021. https://doi.org/10.3390/cryst11060651.
[52] Y.-M. Bahk, K.-H. Kim, G. Ji, K. J. Ahn, D.-S. Kim, and H.-R. Park, "Detection of single nanoparticles inside a single terahertz resonator," *Adv. Photonics Res.*, vol. 3, no. 11, p. 2200134, 2022.
[53] D. Floess, *et al*., "Plasmonic analog of electromagnetically induced absorption leads to giant thin film Faraday rotation of 14°," *Phys. Rev. X*, vol. 7, no. 2, 2017. https://doi.org/10.1103/PhysRevX.7.021048.
[54] S. Han, Y. M. Bahk, N. Park, and D. S. Kim, "Terahertz field enhancement in asymmetric and tapered nano-gaps," *Opt. Express*, vol. 24, no. 3, pp. 2065—2071, 2016.
[55] D. M. Li, *et al*., "Spectroscopic study of gap-surface plasmons in a metallic convex groove array and their applications in nanofocusing and plasmonic sensing," *Phys. Rev. B*, vol. 103, no. 24, 2021. https://doi.org/10.1103/PhysRevB.103.245404.
[56] M. A. Ordal, R. J. Bell, R. W. Alexander, L. L. Long, and M. R. Querry, "Optical-properties of 14 metals in the infrared and far infrared - Al, Co, Cu, Au, Fe, Pb, Mo, Ni, Pd, Pt, Ag, Ti, V, and W," *Appl. Opt.*, vol. 24, no. 24, pp. 4493—4499, 1985.

Supplementary Material: This article contains supplementary material (https://doi.org/10.1515/nanoph-2024-0665).